

# PROGRESS ON SPIN DETECTORS AND SPIN-POLARIZED ELECTRON SCATTERING FROM Na AT NIST

Jabez J. McClelland

Center for Atomic, Molecular, and Optical Physics, NIST, Gaithersburg, MD

Recent progress in the Electron Physics Group at NIST is discussed. Improvements have been made on the low-energy diffuse-scattering spin analyzer, reducing instrumental asymmetries and boosting the effective Sherman function. A figure of merit of  $2.3 \times 10^{-4}$  has been achieved. Thorium has been used as a target in a 100 keV retarding Mott spin analyzer, resulting in an effective Sherman function as high as 0.49. This increased Sherman function, together with an increased scattering intensity, results in a factor of 2 increase in the figure of merit. Good agreement is seen between experiment and theoretical predictions of the Sherman function for thorium. A hierarchical description of the *T*-matrix is discussed as a context for interpreting recent results on spin-polarized electron scattering from optically pumped sodium. Results are presented for elastic and superelastic scattering at 20 eV incident energy.

## 1 Introduction

In this paper, I would like to discuss three separate subjects. Though they may seem somewhat unrelated, they all pertain to the general theme of our work on state-selected electron-atom scattering in the Electron Physics Group at NIST. In the first two sections, I will present some recent work on the improvement of experimental techniques associated with the measurement of electron spin. Innovations in the design of a compact low-energy spin analyzer will be discussed, followed by a description of some recent work on improving the Sherman function of a Mott analyzer by using thorium as a target. In the last section, I will consider some of our latest state-selected results for 20 eV electron scattering from sodium, with particular emphasis on how they contribute to a complete picture of electron-sodium scattering.

## 2 Improved low energy electron spin detector

The low-energy diffuse-scattering electron spin analyzer, developed<sup>1</sup> in the Electron Physics Group at NIST in 1986, has led to significant advancements in the application of polarized electron studies to a large number of fields, including electron microscopy<sup>2</sup> and surface photoemission.<sup>3</sup> The high detection efficiency of the analyzer ( $I/I_0 \sim 0.01$ ), combined with a spin-analyzing power (effective Sherman function  $S_{eff}$ ) of  $\sim 0.1$  leads to a figure of merit  $\mathcal{F} = S_{eff}^2 I/I_0$  of about  $1 \times 10^{-4}$ . This figure of merit is comparable with that of the best Mott detectors. The small size of the detector (about  $10^{-3}m^3$ ) makes this detector an extremely useful tool for a wide

range of applications. Figure 1a shows a sketch of the original detector design. The principle of operation is in essence the same as a conventional Mott detector—the polarized electron beam to be analyzed is incident upon a gold target, and backscattered electrons are collected with two detectors in a plane perpendicular to the component of the polarization to be measured. Two sets of detectors allow measurement of the two transverse components of the spin.

The major difference between this detector and a conventional Mott polarimeter is the ability to operate at a low energy, i.e., 150 eV, instead of 100 keV. In order to make low energy operation possible, the surface of the gold target must be kept clean. This is accomplished by operating the detector in relatively good vacuum ( $\sim 10^{-9}$  Torr), and periodically evaporating a fresh gold film on the target. The high detection efficiency of the detector results from the high backscattering coefficient at 150 eV, and also from the large solid angles collected by the channelplate detectors.

Though the original design of the detector operates quite well, there are two areas in which possibilities for improvement have become evident. The improvements have been incorporated in a new design, which is now in operation.<sup>4</sup>

The first improvement has to do with instrumental asymmetries resulting from the sensitivity of the detector to angular and positional displacements of the incident electron beam. This problem can be particularly troublesome when the detector is used in conjunction with scanning electron microscopy, but is of concern in other applications as well, especially if the source of polarized electrons is not spatially stable. The cause of the sensitivity lies in the angular dependence of the cross section

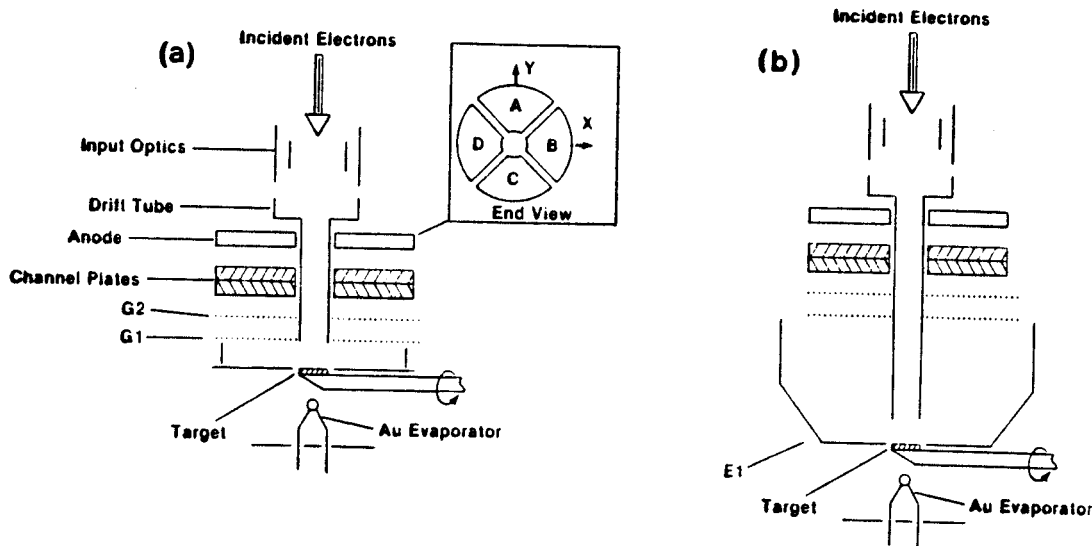


Figure 1. Low-energy diffuse-scattering electron spin analyzer. (a) Original design<sup>1</sup> (G1 = shield grid, G2 = retarding grid) (b) New design,<sup>4</sup> showing negatively biased electrode (E1).

and the variation of the solid angles subtended by the two electron detectors as the beam is displaced.

It was found that, by altering the geometry of the detector and installing suitable optics at the input, instrumental asymmetries could be dramatically reduced. The reduction occurs because the angular dependence of the cross section and the solid angle variation can be made to cancel each other.<sup>5</sup> For example, if a paraxial incident beam passes through a simple einzel lens with focus located between the lens and the target, a spatial displacement of the incident beam is converted at the target into a spatial displacement in the opposite direction plus an angular displacement. The spatial displacement will increase the intensity in the near detector, while reducing it in the far one because of solid angle effects. The angular displacement, however, will decrease the intensity in the near detector and increase it in the far one because the cross section decreases for angles farther from the backscattered direction. By correctly choosing the geometry of the detector, these two effects can be made quite linear over a large range, and so compensation involves a rather simple electron optical design process. In a detector constructed on this principle, using a simple einzel lens, we were able to obtain instrumental asymmetries as low as 0.0035/mm over a displacement of up to 4 mm.

The second improvement concerns optimization of the effective Sherman function of the detector. This was done by careful consideration of the two major influences on the effective Sherman function, i.e., the range of scattering angles over which the channelplate detectors integrate, and the range of inelastic electrons allowed to reach the channelplate detectors.

For 150 eV elastic scattering from an amorphous gold target, the Sherman function generally decreases as one goes closer to scattering in the backward direction. At 180° (full backward direction) it is identically zero by symmetry. Thus the effective Sherman function can be optimized by collecting over a selected interval of backscattering angles, usually not exceeding 150°.

In addition to its angular dependence, the Sherman function has a dependence on the amount of energy lost in scattering from the target. Elastically scattered electrons have the largest Sherman function, while inelastics have a smaller and smaller Sherman function as the energy loss increases. Thus the inclusion of inelastically scattered electrons in the set of detected electrons, though desirable for increasing  $I/I_0$ , tends to decrease the effective Sherman function of the detector. The inelastic window must therefore be carefully controlled to balance the increased collection efficiency against the decrease in  $S_{eff}$ . To accomplish this, the detector is fitted with a retarding grid to optimize the energy range of the inelastic electrons collected.

By examining the original design of the detector (Figure 1a) it is evident that the retarding grid is not optimally designed for either the scattering angle range or the inelastic window. A suboptimal angular range is emphasized, since electrons travelling in the backward direction pass through the grid, while those travelling at smaller scattering angles (closer to 90°) are repelled because their velocity component perpendicular to the grid is reduced by  $\cos \theta$ . Also, because of this angular dependence of the retarding energy, the cut-off energy for inelastically scattered electrons is a strong function of scattering angle, making it impossible to choose a sin-

gle inelastic window for all angles.

These difficulties have been remedied in the new design, shown in Figure 1b, by moving the scattering target further from the channelplate detectors and adding a negatively biased electrode around the target region. With this arrangement, the trajectories of the scattered electrons from a large range of angles are made perpendicular to the retarding grid before passing through it. Thus, all scattering angles are treated more equally by the retarding grid, eliminating the emphasis on low-Sherman-function backscattered electrons, and also providing the same energy window for all scattering angles.

The results of the implementation of the new design features are a Sherman function of up to 0.15 and a figure of merit as high as  $2.3 \times 10^{-4}$ . This represents a significant improvement in the performance of the low energy diffuse-scattering electron spin detector, and will increase its utility in a broad range of fields.

### 3 Use of thorium in a Mott analyzer

As discussed in the preceding section, optimization of electron spin detectors has been a concern in our group recently. To this end, some work has also been done looking for ways to increase the effective Sherman function of a Mott analyzer. If this can be done without a corresponding loss in the detection efficiency  $I/I_0$ , performance of the detector can be dramatically enhanced. Since the figure of merit of a detector is proportional to the square of the effective Sherman function, increasing  $S_{\text{eff}}$  has a much larger potential benefit than increasing the detection efficiency. In addition, a higher  $S_{\text{eff}}$  is advantageous independent of the figure of merit, in that instrumental asymmetries become less significant compared to a larger "real" asymmetry.

Knowing that the physical process underlying the spin sensitivity of Mott detection is the spin-orbit interaction, it is natural to search for a target that has the largest possible spin-orbit effect when electrons scatter from it. Since the spin-orbit interaction increases as the target atomic number  $Z$  gets larger, one is led to look for suitable target materials at the end of the periodic table. Thorium is a high- $Z$  material ( $Z = 90$ ) for which thin target discs are readily available, so we have undertaken a study of the effective Sherman function of a Mott detector using a thorium target.<sup>6</sup> The results of our study are shown in Figure 2. A GaAs polarized electron source was used as a source of polarized electrons, and the Mott detector was of a 100 keV cylindrical design first developed at Rice University.<sup>7</sup> The effective Sherman function was measured for a 0.09 mm thick thorium target as a function of incident electron energy over the range 20–100 keV. An energy window of 25 eV was maintained with suitable retarding voltages at the detectors.

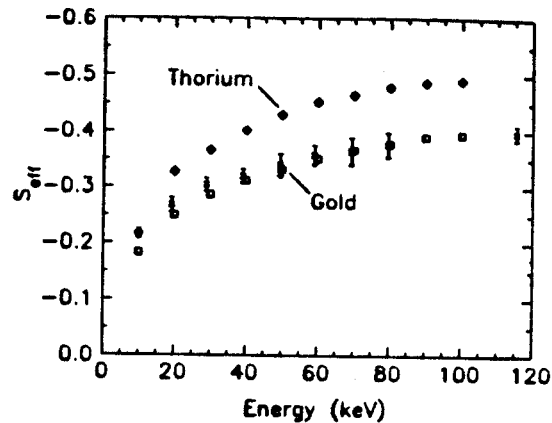


Figure 2. Effective Sherman function  $S_{\text{eff}}$  versus scattering energy. Crosses represent data of Gray *et al.*<sup>8</sup>

Similar measurements were done for a 1250 Å gold foil for comparison with previous gold measurements<sup>8</sup> and the new thorium results. Also done, but not displayed here, were measurements of the dependence of  $S_{\text{eff}}$  on the size of the inelastic window.

The effective Sherman function for the thorium target was found to be significantly higher than it was for the gold. At 100 keV, the gold  $S_{\text{eff}}$  reaches a maximum magnitude of 0.39, while the thorium  $S_{\text{eff}}$  is as high as 0.49. At lower energies, the thorium effective Sherman function is as much as 30% higher. In addition, the scattering intensity for the thorium target was found to be about 15% greater than for the gold target. The combination of these effects results in about a factor of 2 increase in the figure of merit when thorium is used as a target.

Besides improving the effective Sherman function of the Mott analyzer, we were able to provide some interesting comparisons with theory as well. First, our incident electron beam polarization was calibrated with a measurement at 100 keV on the gold target. A value of 0.39 is generally accepted as the correct value for the Sherman function at this energy.<sup>8</sup> This value allowed us to put our gold measurements on an absolute scale, after which they showed agreement with previous retarding Mott measurements,<sup>8</sup> as well as with the recent theory of Ross and Fink.<sup>9</sup>

Comparison could then be made with similar calculations by Ross and Fink for thorium, and excellent agreement was found at 100 keV. The measured value of the Sherman function was  $0.491 \pm 0.009$ , and the theoretical value was 0.485. Though this does not represent a fully independent absolute experimental determination of the Sherman function (a double scattering experiment is required for this), it does show good internal consistency within the theory.

The above mentioned contributions to the advancement of electron-spin polarimetry will hopefully increase the prospects for "complete" electron-atom scattering experiments, in which the polarizations of the incoming electrons, the atomic target, and the scattered electrons are all under experimental control in a single experiment. Given the large body of work in the past year alone on the improvement of spin polarimetry,<sup>4,6,10,11</sup> the future for such experiments seems bright.

#### 4 State-selected electron scattering from sodium at 20 eV

Recently, our ongoing research efforts to study electron scattering from sodium with spin-polarized electrons and atoms have produced a set of elastic scattering data at 20 eV, and a set of superelastic data at 17.9 eV incident energy. These data represent a very extensive (though not yet "complete") set of measurements which yields a broad spectrum of specific information for comparison with theory. Before discussing the results themselves, I would like to outline some thoughts on how measurements of the type we are involved in connect with theoretical calculations.

##### 4.1 The $T$ -matrix

Most state-of-the-art *ab initio* scattering calculations, such as close-coupling calculations, have as their most immediate output a  $T$ -matrix. This matrix, which sometimes takes the form of an  $S$ -matrix or  $K$ -matrix (i.e. reactance matrix), provides the link between an *ab initio* solution of Schrödinger's equation and the prediction of observed scattering intensities. Once a  $T$ -matrix is calculated, scattering intensities are arrived at through complex scattering amplitudes, which are generally expressed as sums over  $T$ -matrix elements with various coefficients, such as Clebsch-Gordan coefficients, spherical harmonics, etc. For example, consider the scattering amplitudes for excitation of the different  $M$ -sublevels in the sodium 3s-3p transition:<sup>\*</sup>

$$f_M^S(\theta, \phi) \propto \sum_{L, l=L \pm 1} i^{L-1} (2L+1)^{1/2} \begin{pmatrix} l & 1 & L \\ -M & M & 0 \end{pmatrix} \times Y_l^{-M}(\theta, \phi) T_l^{S,L}(3s-3p) \quad (1)$$

The  $T$ -matrix itself is a multidimensional matrix with various subscripts corresponding to the different channels in a scattering process. Once the incident energy of the electron is chosen, which then becomes the energy

<sup>\*</sup>This expression is shown for illustrative purposes only. It may prove useful in the upcoming discussion, but the reader is referred to a text on electron scattering<sup>12</sup> for a discussion of all the details.

of the system in the solution to Schrödinger's equation, all the  $T$ -matrix elements corresponding to the various channels can in principle be calculated.

The elements of the  $T$ -matrix can be thought of in a hierarchical sense in order to facilitate keeping the multi-dimensional nature of the matrix in mind (see Figure 3). At the top of the hierarchy are the various energy channels open to the system. These correspond to transitions that may occur in the atomic target. There is a group of elements for each transition energetically allowed, including no transition at all (i.e., elastic scattering). For example, in sodium, we speak of the "3s-3s" channel, the "3s-3p" channel, the "3p-4s" channel, etc.

The next level of the hierarchy corresponds to the spin channels accessible to each transition in the scattering system. There may be only one channel at this level, as would be the case for scattering from a closed shell target such as helium at low energy where spin-orbit effects can be ignored, or there may be several. In the case of low-energy electron scattering from a light one-electron atom, such as hydrogen or an alkali (considered "one-electron" to a good approximation), there are two channels, the singlet and the triplet. These correspond to the two possible relative orientations of the incident electron and the target electron. In heavier atoms, where the spin-orbit interaction becomes significant and  $L-S$  coupling breaks down, there may be more channels. In fact, in this case the separation between this hierarchy level and the next one down becomes less clear. For the present discussion, however, we shall ignore these effects.

The third level of the hierarchy corresponds to a series of orbital angular momentum channels. If no angular momentum is transferred between the electron and the target, this level consists simply of a series of channels corresponding to the partial waves used to describe the scattering. Each channel describes how a partial wave with a particular value of  $L$  scatters from the atom. The set of partial waves is technically infinite, but in practice is usually truncated at some large value of  $L$ .

If, however, angular momentum is transferred between the electron and the target, the angular momentum level of the hierarchy is split into two channels, corresponding to exactly how the angular momentum is transferred. For example, in the case where the atom undergoes an  $S \rightarrow P$  transition, the extra unit of angular momentum can come from the  $L$ th partial wave by changing it into either an  $L+1$  or an  $L-1$  wave, according to the rules of addition of angular momenta. There is a partial wave series for each of these ways in which angular momentum can be transferred.

The  $T$ -matrix, then, has energy level channels, spin channels, and angular momentum channels. In order

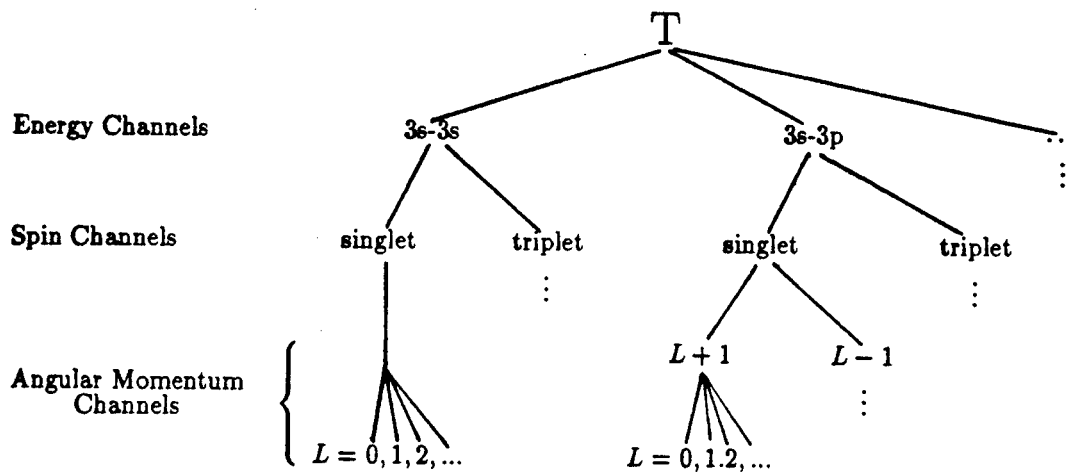


Figure 3.  $T$ -matrix hierarchy for electron-sodium scattering.

to generate a simple total scattering intensity, one must sum over all these channels. Clearly, total scattering intensities do not provide a very exacting test for theoretical predictions. Very real possibilities exist for fortuitous cancellations between the various channels, the result being good agreement between experiment and theory for the wrong reason. The only way to provide a good experimental test of a theoretical approach is to examine all elements of the  $T$ -matrix individually, to the extent that this is possible. This can only be done in state-selected scattering experiments in which all experimental variables are resolved.

Let us examine what experimental techniques can be used to probe the different hierarchies of the  $T$ -matrix. The first level, which consists of the atomic energy level channels, is in part trivial to sort out experimentally. One needs only an energy analyzer on the experiment, which is quite commonplace today. This allows measurement of the ground state elastic channel, as well as the various transition channels connecting the ground state to the excited states of the atom. The first level of the  $T$ -matrix hierarchy, however, contains many more channels than these. For a complete measurement at this level, one must also measure elastic scattering from each of the excited states, as well as inelastic scattering between different excited states. Measuring these cross sections becomes much more difficult, as it usually involves some sort of laser excitation in combination with the electron scattering experiment. Very little experimental work has been done on these other channels,<sup>13,14</sup> though they represent a significant portion of the  $T$ -matrix.

The spin-channel level of the  $T$ -matrix hierarchy has received a great deal of attention lately. The spin of the incident electron can be put under experimental control through the use of a polarized electron source, the spin of

the atomic electron can be manipulated through optical pumping methods, and the spin of the scattered electron can be measured with a Mott polarimeter, as discussed in the first two sections of this paper. A large body of work has been done on investigations involving the role played by the electron spin in scattering,<sup>15</sup> though few true "complete" measurements have been done.

The angular momentum channels in the  $T$ -matrix present somewhat of a problem for experiments. In an ideal world, one would like to be able to measure the scattering process partial wave by partial wave, examining the contribution of each individually. This is generally impossible, though it can be accomplished in a very limited sense by measuring at very low energies where only the first partial wave contributes, or by studying the somewhat analogous process of multiphoton ionization, in which selection rules limit the number of partial waves that can play a role.

By measuring the angular dependence of electron scattering intensities, however, one can obtain most of the partial wave information needed. An angle-resolved intensity is, after all, essentially a "Fourier transform" of the partial wave series, and a complete measurement over the entire angular range can be "back-transformed" to extract the coefficients for each of the individual partial waves. The coefficients are generally complex, though, so some information is lost, but the amount of information obtained is nevertheless quite substantial.

In the situation where angular momentum is transferred between the electron and the target, the angular dependence of the intensity still provides information on the individual partial wave contributions in a "Fourier transform" sense. Now, however, we also have the different transfer channels, e.g.,  $L+1$  and  $L-1$  in a  $\Delta L = 1$  transition. These can be investigated by means of align-

ment and orientation studies. In this type of study, the angular momentum state of the atom is either probed after collision in a coincidence experiment, or prepared before collision in a superelastic scattering experiment. The probabilities of exciting the different  $M$ -sublevels of the excited state, along with phase relations between the corresponding amplitudes, are measured in either case. In the coincidence measurement, the Stokes parameters of the fluorescent light are determined; in the superelastic case the atoms are optically pumped with different light polarizations. The information obtained from these studies relates directly back to the different angular momentum transfer channels in the  $T$ -matrix, by way of some Clebsch-Gordan algebra or perhaps some state-multipole formalism.

It should now be clear what is involved in generating a complete set of measurements which can verify all the predictions of an *ab initio* electron scattering calculation. One needs energy resolution to fix the target excitation channel, spin resolution to fix the spin state of the scattering system, angular resolution to determine the various partial wave contributions, and alignment/orientation information to separate the angular momentum transfer channels. A complete set of measurements entails measuring all possible elastic and inelastic excitation channels, with complete spin and angular momentum resolution. This is certainly a massive task, which any single laboratory or research group can only begin to accomplish. Nevertheless, given the large number of research efforts in this field around the world, it can be reasonably hoped that the combined results will represent significant progress toward this goal.

## 4.2 Experimental results

The foregoing discussion of the  $T$ -matrix has hopefully provided a reasonable context for our most recent results on electron scattering from optically pumped sodium with spin-polarized electrons. For this particular work, we have concentrated on an electron energy of 20 eV, and have measured both elastic scattering from the ground state and superelastic scattering from the first excited state ( $3P$ ). The superelastic results involve measuring de-excitation of the  $3P$ -state in order to obtain alignment and orientation information about the time-inverse inelastic  $3S-3P$  excitation. Thus they were obtained with an incident energy of 17.9 eV in order to make the energy of the electrons after scattering equal to 20 eV (the excitation energy of the  $3P$ -state is 2.1 eV).

Figure 4 shows the elastic scattering results, expressed in terms of a spin asymmetry as a function of scattering angle. This quantity, which highlights the spin dependence in the scattering and hence in the  $T$ -matrix, is determined by measuring intensities with incident and

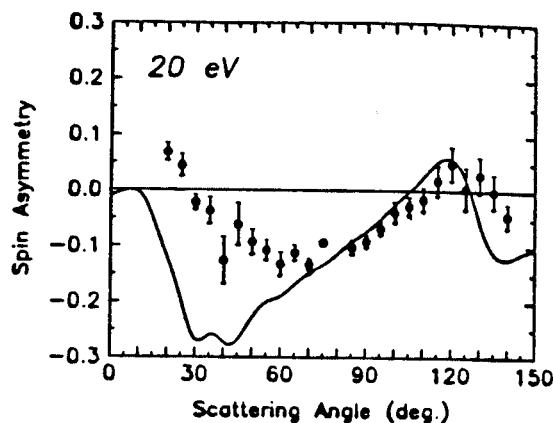


Figure 4. Spin asymmetry for elastic electron scattering from Na at 20 eV. Circles, experiment; solid line, theory of Oza.<sup>16</sup>

atomic spin either parallel or antiparallel to each other. The asymmetry is given by

$$A = P_e^{-1} P_A^{-1} \frac{I_{\uparrow\downarrow} - I_{\uparrow\uparrow}}{I_{\uparrow\downarrow} + I_{\uparrow\uparrow}}, \quad (2)$$

where  $P_e$  and  $P_A$  are the electron and atom beam polarizations, and  $I_{\uparrow\downarrow}$  and  $I_{\uparrow\uparrow}$  are the antiparallel and parallel intensities, respectively. Calculated in this way, the asymmetry is equivalent to a normalized difference between the singlet and triplet scattering cross sections. It can range from a value of  $-1/3$  when the triplet channel dominates, to a value of  $+1$  when singlet dominates. The experimental results in Figure 4 show that at this energy, the scattering is largely triplet over most of the angular range, with a slight singlet dominance at large and small angles.

Also shown in Figure 4 is the spin asymmetry from a 4-state close-coupling calculation of Oza.<sup>16</sup> The agreement between experiment and theory is quite good at large angles, beyond about  $60^\circ$ , but significant differences appear at smaller angles. Below  $30^\circ$ , the theory still predicts a larger triplet cross section, while the experiment indicates that singlet has taken over.

Combined with an absolute determination of the differential cross section for elastic scattering from the sodium ground state, our results provide a nearly complete determination of this energy channel of the  $T$ -matrix. All that is missing is a measurement of the relative phase between the singlet and triplet scattering amplitudes, which must be determined by measuring the spin of the scattered electron while still controlling the atomic and incident electron spins.

Our superelastic results are shown in Figure 5.<sup>17</sup> Since this energy channel involves a  $\Delta L$  of 1, we must concern ourselves not only with the spin channels, but also with the angular momentum transfer channels in the  $T$ -matrix. Thus there is a larger set of parameters

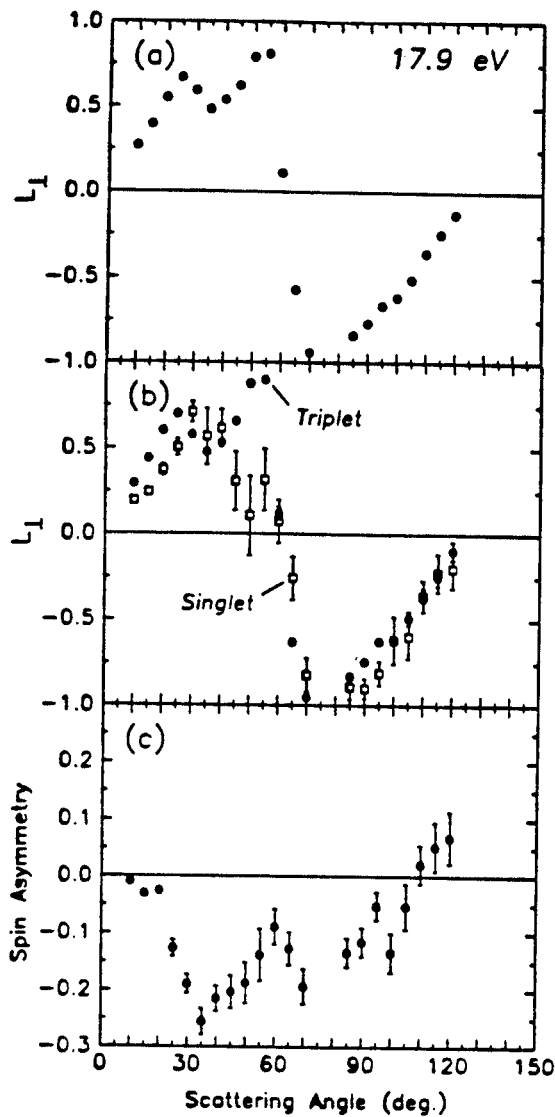


Figure 5. Superelastic electron scattering from Na at 17.9 eV. (a)  $L_{\perp}$  measured with unpolarized electrons. (b)  $L_{\perp}$  separated into singlet and triplet contributions. (c) Spin asymmetry, averaged over  $M_L$ -excitations.

that must be measured in this case. We have followed the tradition of discussing the extra parameters associated with angular momentum transfer in terms of physical quantities describing the atomic wave function.<sup>18</sup> One such quantity is  $L_{\perp}$ , the net angular momentum transferred perpendicular to the scattering plane. By optically pumping with circularly polarized laser light incident perpendicular to the scattering plane, we can conveniently determine  $L_{\perp}$  in terms of the scattering intensities  $I_+$  and  $I_-$  for  $\sigma^+$  and  $\sigma^-$  polarization of the laser:

$$L_{\perp} = \frac{I_+ - I_-}{I_+ + I_-}. \quad (3)$$

Equation 3 shows that  $L_{\perp}$  is a normalized difference

between intensities associated with excitation (or de-excitation) of  $M = \pm 1$  sublevels, and hence contains the necessary angular momentum transfer channel information. Phase difference information, which completes the picture for these channels, is obtained from measurements of  $P_{\text{lin}}$  and  $\gamma$ . These physical parameters result from experiments with linearly polarized light, which we do not consider here.

Figure 5a shows our angle-resolved measurements of  $L_{\perp}$  for 17.9 eV superelastic scattering. The shape of the curve is similar to most measurements of  $L_{\perp}$  in most systems, in that it goes initially positive, crosses over to large negative values at intermediate angles, then increases toward zero at large angles. This particular curve is interesting in that it has a double positive peak at the smaller angles. At present, we do not have a theoretical curve for comparison with our experimental results.

Having separated the angular momentum transfer channels, we must now turn to the spin channels. The singlet and triplet spin channels are still an important part of this inelastic scattering channel, so they must also be resolved. The resolution is expressed by separating  $L_{\perp}$  into singlet and triplet versions  $L_{\perp}^S$  and  $L_{\perp}^T$ , and by determining the spin asymmetry (Equation 2) averaged over angular momentum transfer.<sup>19</sup> This is accomplished experimentally by using spin-polarized incident electrons, and by virtue of the fact that the optical pumping process automatically produces a spin-polarized excited state—spin “up” with  $\sigma^+$  light and spin “down” with  $\sigma^-$  light. The exact expressions for  $L_{\perp}^S$ ,  $L_{\perp}^T$  and  $A$  in terms of scattering intensities are somewhat complicated, so they are not shown here (see Reference 19).  $L_{\perp}^S$  and  $L_{\perp}^T$  both have forms similar to  $L_{\perp}$ ; the complications arise mostly from corrections for incomplete electron beam polarization.

Figure 5b shows the experimental results for  $L_{\perp}^S$  and  $L_{\perp}^T$ . There does not appear to be much of a difference in the way angular momentum is transferred in the two spin channels, except around a scattering angle of 50°. Here we see a prominent peak in  $L_{\perp}^T$ , but no peak in  $L_{\perp}^S$ . This indicates that the second peak in the  $L_{\perp}$  curve of Figure 5a is due entirely to the triplet channel.

Though there is little difference in the way angular momentum is transferred in this inelastic channel, there is quite a large difference in the cross sections for triplet and singlet scattering. This is seen in Figure 5c, which shows the spin asymmetry. In fact, around 30°, the asymmetry almost reaches its maximal value of  $-1/3$ , corresponding to pure triplet scattering. It is also interesting to compare Figure 5c with Figure 4, which shows the spin asymmetry for elastic scattering. The two curves are remarkably similar over the entire angular range, the difference being only that the inelastic curve is generally larger in magnitude and has a little more

structure. This indicates that at this particular energy, the way in which the  $T$ -matrix is partitioned into spin channels is quite similar for the two energy channels.

As was the case for elastic scattering, these superelastic experiments constitute a nearly complete determination of all the accessible experimental information on a particular energy channel in the  $T$ -matrix. When combined with an absolute cross section measurement, the absolute magnitudes of all the relevant scattering amplitudes can be determined. What is missing from the superelastic measurements performed to date is once again phase difference information. Some form of phase differences are measurable by scattering unpolarized electrons from atoms excited with linearly polarized light, but the singlet and triplet contributions cannot be simply extracted from these. Combining spin-polarized incident electrons with linearly polarized optical pumping of the target is not sufficient to extract the necessary information. Measurement of the electron spin after collision, perhaps in combination with elliptically polarized optical pumping not perpendicular to the scattering plane,<sup>19</sup> is necessary for a determination of all the phase differences.

## 5 Conclusion

The elastic and superelastic scattering results presented here represent a concerted effort to learn all there is to know about electron scattering from sodium at a fixed scattering energy of 20 eV. Though there is a great deal of work still to be done, we can at least say that all levels of the  $T$ -matrix (see Figure 3) have been probed in a single batch of measurements. Energy channels, spin channels and angular momentum channels have all been investigated, mostly in a "complete" sense, with the exception of phase difference information.

The two major blocks of work still to be done involve measuring the cross sections for as many of the possible transitions in sodium as possible, and measuring with spin analysis after collision to extract the relative phases of all the various scattering amplitudes. The latter of these awaits significant breakthroughs in the efficiency of spin polarization detectors. The results described in the first two sections of this paper represent our efforts to further the field of spin polarimetry, in the hope that the truly complete experiment will be realizable in the near future.

## 6 Acknowledgements

Major contributions to the work described here have been made by members of the Electron Physics Group at NIST. This work is supported in part by the U.S. De-

partment of Energy, Office of Energy Research, Division of Chemical Sciences.

## References

1. J. Unguris, D.T. Pierce, and R.J. Celotta, *Rev. Sci. Instrum.* **57**, 1314 (1986).
2. D.T. Pierce, J. Unguris, and R.J. Celotta, *MRS Bulletin* **13**, 19 (1988).
3. D.T. Pierce, R.J. Celotta, M.H. Kelley, and J. Unguris, *Nucl. Inst. Meth. A.* **266**, 550 (1988).
4. M.R. Scheinfein, D.T. Pierce, J. Unguris, J.J. McClelland, R.J. Celotta, and M.H. Kelley, *Rev. Sci. Instrum.* **60**, 1 (1989).
5. A. Gellrich, K. Jost, and J. Kessler, in *Electronic and Atomic Collisions, Abstracts of Contributed Papers, ICPEAC XV*, edited by J. Geddes, H.B. Gilbody, A.E. Kingston, C.J. Latimer, and H.R.J. Latimer (1987), page 818.
6. J.J. McClelland, M.R. Scheinfein, and D.T. Pierce, *Rev. Sci. Instrum.* **60**, 683 (1989).
7. L.A. Hodge, T.J. Moravec, F.B. Dunning, and G.K. Walters, *Rev. Sci. Instrum.* **50**, 271 (1979).
8. L.G. Gray, M.W. Hart, F.B. Dunning, and G.K. Walters, *Rev. Sci. Instrum.* **55**, 88 (1984).
9. A. Ross and M. Fink, *Phys. Rev. A* **38**, 6055 (1988).
10. H. Hopster and D.L. Abraham, *Rev. Sci. Instrum.* **59**, 49 (1988).
11. M. Uhrig, A. Beck, J. Goetze, F. Eschen, M. Sohn, G.F. Hanne, K. Jost, and J. Kessler, *Rev. Sci. Instrum.* **60**, 872 (1989).
12. See, e.g., N.F. Mott and H.S.W. Massey, *The Theory of Atomic Collisions*, 3rd edition (Oxford University Press, Oxford, 1965).
13. H.W. Hermann. Ph. D. Thesis, Univ. of Kaiserslautern, 1979.
14. M. Zuo, T.Y. Jiang, L. Vuscovic, and B. Bederson, in *Electronic and Atomic Collisions, Abstracts of Contributed Papers, ICPEAC XVI*, (1989), page 132.
15. J. Kessler, *Polarized Electrons*, 2nd edition (Springer, Berlin, 1985).
16. D.H. Oza, *Phys. Rev. A* **37**, 2721 (1988).
17. J.J. McClelland, M.H. Kelley, and R.J. Celotta. To be published in *Phys. Rev. A*, 1989.
18. N. Anderson, J.W. Gallagher, and I.V. Hertel, *Phys. Rep.* **165**, 1 (1988).
19. I.V. Hertel, M.H. Kelley, and J.J. McClelland, *Z. Phys. D* **6**, 163 (1987).